Available online at www.sciencedirect.com
SCIENCE DIRECT®
ELSEVIER
European Journal of Mechanics B/Fluids 21 (2002) 511–526
EUROPEAN JOURNAL OF MECHANICS B/FLUIDS

The effect of viscosity, surface tension and non-linearity on Richtmyer–Meshkov instability

Pierre Carlès *, Stéphane Popinet

Laboratoire de modélisation en mécanique, Université Pierre et Marie Curie, case 162, 4, place Jussieu, 75252 Paris cedex 05, France

Received 14 February 2002; received in revised form 26 June 2002; accepted 27 June 2002

Abstract

A weakly non-linear theoretical model of the Richtmyer–Meshkov instability between two viscous fluids with surface tension is proposed. The model is based on the application of singular perturbations techniques to the incompressible Navier–Stokes equations written for two superposed immiscible fluids. A simple analytical law of interface deformation is obtained, in which the effects of viscosity, surface tension and non-linearities appear under the form of independent terms. The model gives also access to the velocity and pressure distribution in the fluids, which can be of interest for estimating vorticity diffusion in the fluids. A comparison with accurate direct numerical simulations confirms the validity of the proposed theory. The interface deformation law is then applied to typical experimental configurations in order to estimate the relative influence of surface tension, viscosity and non-linearities on the growth of perturbations for each of the chosen cases.

Keywords: Richtmyer–Meshkov instability; Theoretical; Numerical; Asymptotic expansion; Viscosity

1. Introduction

When a plane shock wave travels across an interface separating two fluids of different densities (or, more precisely, of different acoustic impedances), all perturbations on the interface grow with time and a strong mixing of the two fluids ensues. This instability, named the Richtmyer–Meshkov instability (RM) after it was theoretically predicted by Richtmyer [1] and experimentally observed by Meshkov [2], is involved in numerous physical processes. For instance, it is among the hydrodynamic limiting factors of inertial confinement fusion (see Anderson et al. [3]), and also plays a strong role in the mixing between gases layers in supernovae explosions such as SN 1987A (see Arnett et al. [4]). Recently, Gueyffier and Zaleski [5,6] suggested that the RM instability could play a prominent role in the dynamics of impacts between liquids and liquids or liquids and solids, such as the splashing of a liquid drop on a liquid film or the impact of a wave on a wharf. The RM instability is easy to observe at home, simply by dropping on the floor a bucket full of water: on impacting, the water undergoes a sudden impulsive downward acceleration in the frame of the bucket (stable in the sense of Rayleigh–Taylor), and droplets of water spring out at high velocity as a result of the RM instability on the interface separating air and water.

Simple linear theories written for perfect fluids predict that the growth of perturbations in the RM instability is linear in time, with a rate of growth proportionnal to the wave number of the initial perturbation. In other words, smaller perturbations grow faster than larger ones, but all perturbations grow regardless of their initial dimension (i.e., there is no intrinsic mechanism of mode selection in RM instability). Practically however, several phenomena significantly change this picture. First, when the initial perturbation grows beyond the limit of small interface deformations, non-linear couplings progressively appear which tend to reduce the growth rate, forming the classical ‘spikes and bubbles’ pattern often observed in gravitationnal instabilities.

* Correspondence and reprints.
E-mail address: carles@ccr.jussieu.fr (P. Carlès).

0997-7546/02/$ – see front matter
PII: S0997-7546(02)01199-8

Also, surface tension between the two fluids reduces the linear rate of growth by opposing to the interface deformation. Finally, viscous stresses inside and between the fluids also tend to slow down the interface deformation. The common characteristic of these three mechanisms is to act preferentially on the smaller perturbations: hence the perturbations with the fastest initial growth are also those on which non-linearities, surface tension and viscosity have the strongest impact; on the contrary, large initial perturbation, despite their slow initial rate of growth, progressively tend to overcome the smaller ones, being mostly unaffected by the three mechanisms listed above. As a consequence, predicting the time evolution of a given initial perturbation is a complex task which involves knowing how these three mechanisms affect the initial growth of perturbations. Although each of these factors has been studied separately (see Mikaelian [7,8], Zhang and Sohn [9], Velikovich and Dimonte [10]), no theoretical work has been made up to now on their relative influence when the three are present together. Moreover, as will be seen later, the only existing theoretical prediction of the effect of viscosity on the RM instability (Mikaelian [8]) does not seem to agree with direct numerical simulations. In this context, the aim of the study presented in this paper is to extend and complement a first analysis recently published (Carlès and Popinet [11]), in which only viscosity and non-linear couplings were considered. In the present work, an analytical theory of the RM instability between two fluids of arbitrary properties is provided which includes the effects of viscosity, surface tension and weak non-linearities in a quantitative and accurate way. The analytical method used here and its limitations are discussed in details, and the predictions of the model are applied in a systematised way to classical experimental results.

The theoretical models of the RM instability can be sorted in two classes: the compressible and incompressible ones. In the compressible models, the two fluids are described as compressible inviscid fluids (i.e., they follow Euler's equations), and the equations are linearised for small perturbations around a base flow corresponding to the travelling of a plane wave across a plane interface between two fluids of different properties (usually two gases of different adiabatic indices). These equations give access to the linear growth of the initial perturbations of the interface as the shock crosses it. Such models where used by several authors in the past to predict the behaviour of the interface for different pairs of gases and different strengths of shock waves (see, for instance, Richtmyer [1], Yang et al. [12], Velikovich [13], Wouchuk and Nishihara [14]). Although this technique has proven efficient in predicting the early response of the interface to the passage of the shock wave, it is very difficult to extend to the non-linear regime. As a consequence, the predictions based on linearised compressible models always fail after some time, when the deformation of the interface becomes too large for non-linear effects to be negligible.

In the case of incompressible models, the compressibility of the fluids is neglected and the passage of the shock wave is assimilated to a brief but strong acceleration applied to both fluids. The RM instability is thus seen as a particular case of Rayleigh–Taylor instability in which the gravitational acceleration is impulsive instead of constant (hence the name 'Impulsive Models' given to this class of models). Richtmyer [1] was the first to introduce this analogy, and the predictions of the impulsive models have proven in good quantitative agreement with those of compressible models, at least in the case of weak incident shocks. The main advantage of impulsive models is of course their increased simplicity compared to compressible ones: they can be more easily extended to include effects such as surface tension (Mikaelian [7]), viscosity (Mikaelian [8]) or non-linear couplings between perturbations (see Zhang and Sohn [9], Velikovich and Dimonte [10], Berning and Rubenchik [15]). The main drawback is of course a bad description of the flow at early times, usually resulting in an over-estimation of the maximum velocity of the interface.

Over the years, several authors have clearly identified the parametric domains where the predictions of impulsive models are in good agreement with those of compressible ones, sometimes proposing ad hoc corrections to extend their validity beyond these boundaries (see Meyer and Blewett [16], Mikaelian [17], Yang et al. [12], Wouchuk and Nishihara [14], Vandenboomgaerde et al. [18], Hurricane et al. [19]). Zhang and Sohn [20] finally bridged the gap between the two classes of models by showing that a uniformly valid description of the time law for the interface deformation could be obtained using matched asymptotic expansions in time, based on a compressible model at early times and an impulsive one at late times. Their approach was recently very elegantly simplified by Vandenboomgaerde et al. [21], yielding a very convenient high-order non-linear model for predicting the interface growth between inviscid fluids.

It is thus now clear that the effect of compressibility on the RM instability is limited to the early times of the interface evolution and that its subsequent deformation follows approximately incompressible equations, a conclusion recently confirmed by the numerical simulations performed by Kotelnikov et al. [22].

In the present work, our aim is to weigh the relative influence of non-linearities, surface tension and viscosity on this subsequent incompressible deformation of the interface, by proposing an impulsive model which includes all these effects at first order in a 2D geometry. In Section 2, the governing equations of the problem are first presented and made non-dimensional, and their asymptotic analysis is then detailed. In Section 3, the predictions obtained through the asymptotic analysis are validated against a set of direct numerical simulations we performed using a front-tracking code designed in our laboratory. The theoretical model is discussed and applied to several experimental cases in Section 4, and the paper is finally concluded in Section 5.

2. Theoretical model

2.1. The system under study

The system under study is the superposition of two non-miscible viscous incompressible fluids, infinite in lateral and vertical extension. The fluids are separated by an interface with surface tension on which a bidimensional sinusoidal perturbation is initially present. At a given time (taken as the origin of the time variable), the system is subjected to a sudden and very brief acceleration $g(t)$, and the evolution of the fluid flow and of the interface deformation is studied. A schematic representation of the initial set-up is given in Fig. 1 (the x-axis is in the plane of the non-perturbed interface, the z-axis perpendicular to it and oriented in the opposite direction to that of the impulsive acceleration). As is customary in impulsive models, the time-dependent acceleration is represented by a Dirac function, under the form:

$$g(t) = \Delta V\, \delta(t),$$

where ΔV is the speed change imparted to the fluids by the shock. The equation of the interface is defined by function η, under the form:

$$z = \eta(x, t).$$

Initially, η is purely sinusoidal:

$$\eta(x, t = 0) = \eta_0 \cos(kx).$$

The following set of non-dimensional parameters and variables is defined (with $(u^{(i)}, w^{(i)})$ the components of the velocity of fluid (i), $P^{(i)}$ the pressure and $\rho^{(i)}$ the density):

$$u'^{(i)} = \frac{u^{(i)}}{\Delta V}, \qquad w'^{(i)} = \frac{w^{(i)}}{\Delta V}, \qquad P'^{(i)} = \frac{P^{(i)}}{(\rho^{(1)} + \rho^{(2)})\Delta V^2},$$
$$x' = kx, \qquad z' = kz, \qquad t' = k\Delta V\, t.$$

Using the above parameters, the Navier–Stokes incompressible unsteady equations become (subscripts indicate partial derivatives and primes ($'$) have been omitted):

$$u_x^{(i)} + w_z^{(i)} = 0, \tag{i.1}$$

$$u_t^{(i)} + u^{(i)}u_x^{(i)} + w^{(i)}u_z^{(i)} = -\frac{\rho^{(1)} + \rho^{(2)}}{\rho^{(i)}} P_x^{(i)} + \frac{1}{\mathrm{Re}^{(i)}}\left(u_{xx}^{(i)} + u_{zz}^{(i)}\right), \tag{i.2}$$

$$w_t^{(i)} + u^{(i)}w_x^{(i)} + w^{(i)}w_z^{(i)} = -\frac{\rho^{(1)} + \rho^{(2)}}{\rho^{(i)}} P_z^{(i)} + \frac{1}{\mathrm{Re}^{(i)}}\left(w_{xx}^{(i)} + w_{zz}^{(i)}\right) - \delta(t), \tag{i.3}$$

$\mathrm{Re}^{(i)}$ is the Impulsive Reynolds number, defined as:

$$\mathrm{Re}^{(i)} = \frac{\Delta V\, \rho^{(i)}}{\mu^{(i)} k},$$

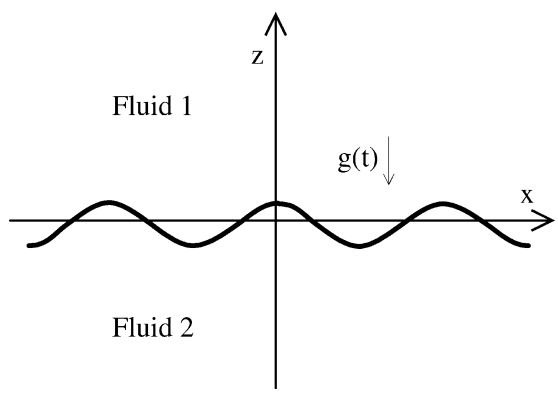

Fig. 1. Initial set-up.

where $\mu^{(i)}$ and $\rho^{(i)}$ are the viscosity and the density of fluid (i). Note that in the above equations, $\delta(t)$ now stands for the non-dimensional Dirac function (the primes have been omitted). To the above equations are added seven non-dimensional boundary conditions (where the primes have again been omitted):

For $z' = (k\eta_0)\eta'$ (i.e., on the interface):

$$\eta_t = \frac{1}{k\eta_0} w^{(i)} - \eta_x u^{(i)}, \tag{C1}$$

$$u^{(1)} = u^{(2)}, \tag{C2}$$

$$w^{(1)} = w^{(2)}, \tag{C3}$$

$$u_z^{(1)} + w_x^{(1)} = \frac{\mu^{(2)}}{\mu^{(1)}}\left(u_z^{(2)} + w_x^{(2)}\right), \tag{C4}$$

$$P^{(1)} - \frac{2\rho^{(1)}}{\rho^{(1)}+\rho^{(2)}} \frac{1}{\mathrm{Re}^{(1)}} w_z^{(1)} - \frac{k\eta_0}{We}\eta_{xx} = P^{(2)} - \frac{2\rho^{(2)}}{\rho^{(1)}+\rho^{(2)}} \frac{1}{\mathrm{Re}^{(2)}} w_z^{(2)}. \tag{C5}$$

For $z' \to \infty$ (i.e., high above the interface, in fluid (1)):

$$P_z^{(1)} \to -\frac{\rho^{(1)}}{\rho^{(1)}+\rho^{(2)}}\delta(t). \tag{C6}$$

For $z' \to -\infty$ (i.e., far below the interface, in fluid (2)):

$$P_z^{(2)} \to -\frac{\rho^{(2)}}{\rho^{(1)}+\rho^{(2)}}\delta(t). \tag{C7}$$

Condition (C1) represents the fact that the interface is a material surface. Conditions (C2), (C3) express the continuity of the velocity accross the interface, while conditions (C4), (C5) express the continuity of the stress tensor. Conditions (C6), (C7) are a consequence of the vanishing of the velocity far from the interface: the pressure gradient tends to become purely hydrostatic. In the above conditions, *We* represents the Impulsive Weber number, defined as:

$$We = \frac{(\rho^{(1)}+\rho^{(2)})\Delta V^2}{\sigma k}$$

with σ the surface tension between the two fluids. The initial conditions associated with this system are the absence of motion before the impulsive acceleration takes place ($u^{(i)} = w^{(i)} = 0$) and a sinusoidal deformation of the interface (i.e., $\eta(x, t=0) = \cos(x)$ in non-dimensional form).

2.2. Asymptotic analysis

2.2.1. The asymptotic conditions

As usual in such analysis, the perturbations of the interface are initially assumed to be small, which reads:

$$\varepsilon = (k\eta_0) \ll 1. \tag{1}$$

However, even with the assumption of small initial perturbations, the explicit resolution of systems (1.1)–(1.3) and (2.1)–(2.3) is impossible for arbitrary values of the Reynolds numbers $\mathrm{Re}^{(1)}$ and $\mathrm{Re}^{(2)}$. Examination of the usual experimental configuration for RM experiments shows that these Impulsive Reynolds numbers are generally much larger than 1. For instance, Reynolds numbers in experiments with gases in shock tubes range from a few thousands (see Vetter and Sturtevant [23]) to more than 15 000 (see Jones and Jacobs [24]). In experiments with impulsively accelerated liquid pairs such as Jacobs and Sheeley's or Jacobs and Niederhaus' experiments [25,26], values between 1000 and 100 000 are witnessed. Finally, even in the case of a falling bucket of water, the smaller Reynolds number of the two ($\mathrm{Re}^{(1)}$ in air) is still often larger than 50 for perturbations no smaller than 1 mm. Consequently, in all relevant cases, $\mathrm{Re}^{(1)}$ and $\mathrm{Re}^{(2)}$ can be assumed larger than 1, which greatly simplifies the problem.

Non-viscous linear theories show that the impulsive gravity drives a motion of the fluids in which the tangential velocity is periodically discontinuous across the interface. This is what would be obtained with systems (1.1)–(1.3) and (2.1)–(2.3) if $\mathrm{Re}^{(1)}$ and $\mathrm{Re}^{(2)}$ where taken infinite. In viscous fluids on the contrary, viscous stresses force the velocity to be continuous across the interface: the vorticity deposited at the interface by the impulsive gravity (or the shock) progressively diffuses into the fluids. For large values of $\mathrm{Re}^{(1)}$ and $\mathrm{Re}^{(2)}$, this viscous diffusion remains slow and is limited to a close vicinity of the deformed interface, where strong velocity shears are observed: two boundary layers appear on each side of the interface. The system is thus singular: neglecting viscosity altogether in (1.1)–(1.3) and (2.1)–(2.3) contradicts boundary conditions (C2), (C3), which makes necessary the introduction of boundary layers where viscous effects are not neglected.

In the calculation presented here, the following scaling for the Reynolds numbers is considered:

$$\mathrm{Re}^{(i)} = \frac{R^{(i)}}{\varepsilon^2} \quad \text{with } R^{(i)} = \mathrm{O}(1). \tag{2}$$

A detailed asymptotic analysis shows that such a choice, among all the possible scalings for large Reynolds numbers, leads to the most descriptive expansion (i.e., values of $\mathrm{Re}^{(i)}$ smaller or larger than ε^{-2} , provided they remain larger than 1, would lead to systems which are particular cases of the expansions obtained for $\mathrm{Re}^{(i)}$ of order ε^{-2}). Although this scaling can be obtained formally by applying the so-called Least Degeneracy Principle [27] to the asymptotic equations, the same conclusion can be reached on purely physical grounds: the choice of $\mathrm{Re}^{(i)} = \mathrm{O}(\varepsilon^{-2})$ leads indeed to a boundary layer thickness of the same order as the interface deformation (i.e., ε). For larger values of $\mathrm{Re}^{(i)}$, the boundary layer is smaller than the interface deformation and the curvature of the interface is neglected in the calculation of the viscous effects, which is a particular case. For smaller values of $\mathrm{Re}^{(i)}$ on the contrary, the boundary layer is too thick to be influenced by the interface deformation: the boundary layer system remains unable to accommodate for the continuity of velocity and stress tensor at the interface, and the singular nature of the interface is not resolved.

Finally, a question remains as regards the order of magnitude of *We*, the Impulsive Weber Number. In experiments with pairs of miscible gases or liquids, no surface tension is present: *We* is infinite. In the case of an interface between air and water and an impact velocity of a few meters per seconds, *We* ranges from 50 (for 1 mm perturbations) to 5000 (for 10 cm perturbations). It is again tempting to assume that *We* is much larger than 1, and make an asymptotic treatment of surface tension like was made for viscosity. But assuming $We \gg 1$, as will be seen in what follows, leads to a monotonic correction of the interface deformation law which poorly describes the intrinsically periodic nature of the motion of interfaces with surface tension. It is possible to calculate a general solution of our system for arbitrary Weber numbers, but such a calculation is extremely intricate, with little real benefit: indeed, parametric analysis shows that when the asymptotic solution for large Weber numbers fails (as it does when time elapses), the perturbations have usually grown to a point where it is no longer relevant to assume that the deformation of the interface is small (in the sense of condition (1)). Consequently, there are other assumptions which fail at the same time as the asymptotic expansion for large *We*. A general calculation for arbitrary *We* would thus be a purely formal exercise. As a consequence, the following scaling will be chosen for *We* in what follows:

$$We = \frac{W}{\varepsilon} \quad \text{with } W = \mathrm{O}(1). \tag{3}$$

With such a choice, the correction to the interface deformation due to surface tension is of the same order as the corrections due to viscosity and non-linearities.

Conditions (1)–(3) are the asymptotic conditions applied to systems (1.1)–(1.3) and (2.1)–(2.3) for the resolution of the problem.

2.2.2. Asymptotic analysis at first order

Two domains are considered in each fluid: the external domain (far from the interface) and the boundary layer. The equations in each domain are obtained using the technique of Matched Asymptotic Expansions (see Kevorkian and Cole [27]).

(a) External domain: The equations in the external domain are obtained by introducing conditions (1)–(3) into Eqs. (1.1)–(1.3) and (2.1)–(2.3), and making ε go to zero for fixed t, x and z. The following expansions are considered:

$$\begin{aligned} u^{(i)} &= \varepsilon \bar{u}^{(i)} + \mathrm{O}\big(\varepsilon^2\big), \\ w^{(i)} &= \varepsilon \overline{w}^{(i)} + \mathrm{O}\big(\varepsilon^2\big), \\ P^{(i)} &= \Pi^{(i)} + \varepsilon \overline{P}^{(i)} + \mathrm{O}\big(\varepsilon^2\big), \end{aligned}$$

where $\bar{u}^{(i)}$, $\overline{w}^{(i)}$, $\Pi^{(i)}$ and $\overline{P}^{(i)}$ are order one functions of x, z and t. $\Pi^{(i)}$ is the hydrostatic component of the non-dimensional pressure, defined as:

$$\Pi^{(i)} = -\frac{\rho^{(i)}}{\rho^{(1)} + \rho^{(2)}} \delta(t) z.$$

The following equations are obtained:

$$\begin{aligned} &\bar{u}_x^{(i)} + \overline{w}_z^{(i)} = 0, \\ &\bar{u}_t^{(i)} = -\frac{\rho^{(1)} + \rho^{(2)}}{\rho^{(i)}} \overline{P}_x^{(i)}, \\ &\overline{w}_t^{(i)} = -\frac{\rho^{(1)} + \rho^{(2)}}{\rho^{(i)}} \overline{P}_z^{(i)}. \end{aligned} \tag{i.4}$$

(b) Boundary layers: The equations in the boundary layers are obtained by introducing conditions (1)–(3) into Eqs. (1.1)–(1.3) and (2.1)–(2.3), and making ε go to zero for fixed t, x and $\tilde{z}$, with $\tilde{z}$ the boundary layer variable defined as:

$$\tilde{z} = \frac{z}{\varepsilon}.$$

The following expansions are considered:

$$\begin{aligned} u^{(i)} &= \varepsilon \tilde{u}^{(i)} + \mathrm{O}\big(\varepsilon^2\big), \\ w^{(i)} &= \varepsilon \widetilde{w}^{(i)} + \mathrm{O}\big(\varepsilon^2\big), \\ P^{(i)} &= \varepsilon \widetilde{P}^{(i)} + \mathrm{O}\big(\varepsilon^2\big), \end{aligned}$$

where $\tilde{u}^{(i)}$, $\widetilde{w}^{(i)}$ and $\widetilde{P}^{(i)}$ are order one functions of x, $\tilde{z}$ and t. The following equations are obtained:

$$\begin{aligned} \widetilde{w}^{(i)}_{\tilde{z}} &= 0, \\ \tilde{u}^{(i)}_t + \widetilde{w}^{(i)} \tilde{u}^{(i)}_{\tilde{z}} &= -\frac{\rho^{(1)} + \rho^{(2)}}{\rho^{(i)}} \widetilde{P}^{(i)}_x + \frac{1}{R^{(i)}} \tilde{u}^{(i)}_{\tilde{z}\tilde{z}}, \\ \widetilde{P}^{(i)}_{\tilde{z}} &= -\frac{\rho^{(i)}}{\rho^{(1)} + \rho^{(2)}} \delta(t). \end{aligned} \tag{i.5}$$

The boundary conditions applied to systems (1.5) and (2.5) on the interface are the physical conditions (C2)–(C5). The boundary condition applied to system (1.4) for $z \to \infty$ is the physical condition (C6), while the boundary condition applied to system (2.4) for $z \to -\infty$ is the physical condition (C7). The matching conditions between external and boundary layer systems (i.4) and (i.5) is obtained by insuring that the behaviour of any boundary layer parameter $\widetilde{X}$ when $\tilde{z}$ goes to infinity is asymptotically equivalent to the behaviour of the corresponding external parameter $\overline{X}$ when z goes to zero (see [27]). The link between the equation of the interface and the fluids flow is finally obtained through condition (C1).

(c) Solutions: Using separation of variables between x and z (or $\tilde{z}$) and Laplace transforms to solve the four systems (i.4) and (i.5) for the corresponding boundary and matching conditions, the following first-order solutions are found:

External solutions in fluid (1):

$$\begin{aligned} \overline{u}^{(1)} &= A\,\mathrm{e}^{-z} \sin(x), \\ \overline{w}^{(1)} &= A\,\mathrm{e}^{-z} \cos(x), \\ \overline{P}^{(1)} &= \frac{\rho^{(1)}}{\rho^{(1)} + \rho^{(2)}} A\delta(t)\,\mathrm{e}^{-z} \cos(x). \end{aligned} \tag{1.6}$$

External solutions in fluid (2):

$$\begin{aligned} \overline{u}^{(2)} &= -A\,\mathrm{e}^{+z} \sin(x), \\ \overline{w}^{(2)} &= A\,\mathrm{e}^{+z} \cos(x), \\ \overline{P}^{(2)} &= -\frac{\rho^{(2)}}{\rho^{(1)} + \rho^{(2)}} A\delta(t)\,\mathrm{e}^{+z} \cos(x). \end{aligned} \tag{2.6}$$

Boundary layer solutions in fluid (1):

$$\begin{aligned} \tilde{u}^{(1)} &= A\left[1 - \frac{2\mu^{(2)}\sqrt{R^{(2)}}}{\mu^{(1)}\sqrt{R^{(1)}} + \mu^{(2)}\sqrt{R^{(2)}}} \operatorname{erfc}\left(\frac{z^*\sqrt{R^{(1)}}}{2\sqrt{t}}\right)\right] \sin(x), \\ \widetilde{w}^{(1)} &= A\cos(x), \\ \widetilde{P}^{(1)} &= \frac{\rho^{(1)}}{\rho^{(1)} + \rho^{(2)}} \delta(t)\big[A\cos(x) - \tilde{z}\big]. \end{aligned} \tag{1.7}$$

Boundary layer solutions in fluid (2):

$$\begin{aligned}
\tilde{u}^{(2)} &= A\left[\frac{2\mu^{(1)}\sqrt{R^{(1)}}}{\mu^{(1)}\sqrt{R^{(1)}}+\mu^{(2)}\sqrt{R^{(2)}}}\operatorname{erf c}\left(-\frac{z^*\sqrt{R^{(2)}}}{2\sqrt{t}}\right)-1\right]\sin(x),\\
\widetilde{w}^{(2)} &= A\cos(x),\\
\widetilde{P}^{(2)} &= -\frac{\rho^{(2)}}{\rho^{(1)}+\rho^{(2)}}\delta(t)\big[A\cos(x)+\tilde{z}\big].
\end{aligned} \tag{2.7}$$

In the above solutions, A stands for the Atwood number:

$$A=\frac{\rho^{(1)}-\rho^{(2)}}{\rho^{(1)}+\rho^{(2)}}$$

and z^* is the vertical space variable in the boundary layers, measured relatively to the interface:

$$z^*=\tilde{z}-\eta.$$

The equation of the interface is obtained using solutions (i.6) and (i.7) and the materiality condition (C1):

$$\eta=(1+At)\cos(x)+\mathrm{O}(\varepsilon). \tag{4}$$

The above expression is the classical first-order linear solution for the interface equation in the impulsive model. Note however that even at this order of expansion, the velocity field is affected by the presence of viscous stresses (see solutions (i.7)).

2.2.3. Asymptotic analysis at second order

For the chosen set of asymptotic conditions (1)–(3), the effect of viscosity, surface tension and non-linearity on the law of interface deformation appears at the second order of expansion in ε. The expansion is extended to order ε^2:

External expansions:

$$\begin{aligned}
u^{(i)} &= \varepsilon\overline{u}^{(i)}+\varepsilon^2\overline{\overline{u}}^{(i)}+\mathrm{O}\big(\varepsilon^3\big),\\
w^{(i)} &= \varepsilon\overline{w}^{(i)}+\varepsilon^2\overline{\overline{w}}^{(i)}+\mathrm{O}\big(\varepsilon^3\big),\\
P^{(i)} &= \Pi^{(i)}+\varepsilon\overline{P}^{(i)}+\varepsilon^2\overline{\overline{P}}^{(i)}+\mathrm{O}\big(\varepsilon^3\big),
\end{aligned}$$

($\overline{\overline{u}}^{(i)}$, $\overline{\overline{w}}^{(i)}$ and $\overline{\overline{P}}^{(i)}$ are order one functions of x, z and t).

External equations:

$$\begin{aligned}
\overline{\overline{u}}^{(i)}_x+\overline{\overline{w}}^{(i)}_z &= 0,\\
\overline{\overline{u}}^{(i)}_t &= -\frac{\rho^{(1)}+\rho^{(2)}}{\rho^{(i)}}\overline{\overline{P}}^{(i)}_x,\\
\overline{\overline{w}}^{(i)}_t+\overline{u}^{(i)}\overline{w}^{(i)}_x+\overline{w}^{(i)}\overline{w}^{(i)}_z &= -\frac{\rho^{(1)}+\rho^{(2)}}{\rho^{(i)}}\overline{\overline{P}}^{(i)}_z.
\end{aligned} \tag{i.8}$$

Boundary layers expansions:

$$\begin{aligned}
u^{(i)} &= \varepsilon\tilde{u}^{(i)}+\varepsilon^2\tilde{\tilde{u}}^{(i)}+\mathrm{O}\big(\varepsilon^3\big),\\
w^{(i)} &= \varepsilon\widetilde{w}^{(i)}+\varepsilon^2\widetilde{\widetilde{w}}^{(i)}+\mathrm{O}\big(\varepsilon^3\big),\\
P^{(i)} &= \varepsilon\widetilde{P}^{(i)}+\varepsilon^2\widetilde{\widetilde{P}}^{(i)}+\mathrm{O}\big(\varepsilon^3\big),
\end{aligned}$$

($\tilde{\tilde{u}}^{(i)}$, $\widetilde{\widetilde{w}}^{(i)}$ and $\widetilde{\widetilde{P}}^{(i)}$ are order one functions of x, $\tilde{z}$ and t).

Boundary layers equations:

$$\begin{aligned}
\widetilde{w}^{(i)}_{\tilde{z}} &= -\tilde{u}^{(i)}_x,\\
\tilde{u}^{(i)}_t+\tilde{u}^{(i)}\tilde{u}^{(i)}_x+\widetilde{w}^{(i)}\tilde{u}^{(i)}_{\tilde{z}}+\widetilde{\widetilde{w}}^{(i)}\tilde{u}^{(i)}_{\tilde{z}} &= -\frac{\rho^{(1)}+\rho^{(2)}}{\rho^{(i)}}\widetilde{\widetilde{P}}^{(i)}_x+\frac{1}{R^{(i)}}\tilde{u}^{(i)}_{\tilde{z}\tilde{z}},\\
\widetilde{\widetilde{P}}^{(i)}_{\tilde{z}} &= -\frac{\rho^{(i)}}{\rho^{(1)}+\rho^{(2)}}\widetilde{w}^{(i)}_t.
\end{aligned} \tag{i.10}$$

The same procedure as for the first order is used to solve the systems at second order, with the same physical and matching conditions. The calculation is extremely involved, requiring typically more than a hundred pages. In order to avoid excessive complications, the solutions at second order will not be detailed. Only the resulting law of interface deformation is presented:

$$\begin{aligned}
\eta &= h + \varepsilon\widetilde{h} + \mathrm{O}(\varepsilon^2),\\
h &= (1+At)\cos(x),\\
\widetilde{h} &= -\frac{1}{W}\left(\frac{1}{2}t^2+\frac{1}{6}t^3\right)\cos(x) - \frac{8A}{3\sqrt{\pi}}t^{3/2}\left(\frac{\rho^{(2)}}{\rho^{(1)}+\rho^{(2)}}\frac{1}{\sqrt{R^{(2)}}}\frac{\mu^{(1)}\sqrt{R^{(1)}}}{\mu^{(1)}\sqrt{R^{(1)}}+\mu^{(2)}\sqrt{R^{(2)}}}\right.\\
&\quad\left.+\frac{\rho^{(1)}}{\rho^{(1)}+\rho^{(2)}}\frac{1}{\sqrt{R^{(1)}}}\frac{\mu^{(2)}\sqrt{R^{(2)}}}{\mu^{(1)}\sqrt{R^{(1)}}+\mu^{(2)}\sqrt{R^{(2)}}}\right)\cos(x) - \frac{1}{2}A^3t^2\cos(2x).
\end{aligned} \tag{5}$$

2.2.4. The law of interface deformation

Translating (5) in dimensional variables leads to the weakly non-linear law of interface deformation for the RM instability between two viscous fluids with surface tension:

$$\begin{aligned}
\frac{\eta}{\eta_0}(x,t) &= (1+A\Delta V\,kt)\cos(kx)\\
&\quad - \frac{16}{3\sqrt{\pi}}\frac{\sqrt{\rho^{(1)}\mu^{(1)}}\sqrt{\rho^{(2)}\mu^{(2)}}}{(\rho^{(1)}+\rho^{(2)})(\sqrt{\rho^{(1)}\mu^{(1)}}+\sqrt{\rho^{(2)}\mu^{(2)}})}A\Delta V\,k^2t^{3/2}\cos(kx)\\
&\quad - \frac{\sigma}{2(\rho^{(1)}+\rho^{(2)})}k^3t^2\left(1+\frac{1}{3}A\Delta V\,kt\right)\cos(kx)\\
&\quad - \frac{1}{2}\eta_0A^3\Delta V^2\,k^3t^2\cos(2kx).
\end{aligned} \tag{6}$$

Several points can be noted. First, each effect (viscosity, surface tension and non-linearity) appears under the form of a specific term corresponding to an attenuation of the linear growth rate (the first term of Eq. (6)). Owing to the assumption of large Reynolds and Weber numbers, coupled phenomena between these three effects do not appear at the chosen order of expansion (ε^2). In other words, the viscous or capillary attenuation of the non-linear term (fourth term in Eq. (6)) would only appear if the expansion was pursued to third order in ε (i.e., ε^3), a calculation which would probably be too complex to yield any practical result. One should thus expect the nonlinear term to be the same as in the non-viscous case, which is indeed the case (see, for instance, Zhang and Sohn [20] for a comparison). This constitutes a first indirect validation of the whole calculation. Then, one can note that the correction due to surface tension (third term in Eq. (6)) is monotonic in time, whereas it should be periodic for arbitrary Weber numbers. This is a consequence of the fact that the equations were expanded for large Weber numbers: the obtained term is a second-order expansion of the exact periodic solution in the linear regime (as can be verified in a straightforward manner). As stressed before, a general calculation for arbitrary Weber numbers would be possible, but of limited interest: for typical experimental parameters, the hypothesis of small interface deformation fails much before the first oscillation has taken place, so that Eq. (5) becomes invalid anyway. For the time range of validity of expansion (5) (a point which will be discussed later in the text), the expansion for large Weber numbers is a very good approximation of the exact solution. Finally, one could wonder why the predicted viscous correction in Eq. (6) vanishes in the case of a one-fluid viscous system (i.e., $\rho^{(1)}=0$ or $\mu^{(1)}=0$), whereas it is known (in the Rayleigh–Taylor case for instance) that viscosity still plays a role even when only one fluid is present. The reason is that, in this latter case, no boundary layer is present and the viscous correction comes from the flow in the external domains of fluid. It can easily be shown that viscosity in the external domains only influences the interface deformation at order ε^2, so that Eq. (5) remains valid: the viscous contribution to the interface deformation at order ε (coming from the boundary layers) is zero.

In [8], Mikaelian proposed an expression for the linear RM instability between two viscous fluids. His method was based on moment equations applied to a non-viscous approximation of the vertical velocity, and lead to the following law of interface deformation:

$$\frac{\eta}{\eta_0}(x,t) = \left(1+A\Delta V\frac{1-\mathrm{e}^{-2k^2\nu t}}{2k\nu}\right)\cos(kx) \quad \text{with } \nu = \frac{\mu^{(1)}+\mu^{(2)}}{\rho^{(1)}+\rho^{(2)}}. \tag{7}$$

The expansion of this law for small times yields:

$$\frac{\eta}{\eta_0}(x,t) = (1+A\Delta V\,kt)\cos(kx) - A\Delta V\,k^3\nu t^2\cos(kx),$$

which should be compared to the first two terms of expression (6). The difference is both qualitative and quantitative: the power law in time is different, and for most cases the two expressions for the viscous correction differ by several orders of magnitude. As the two predictions are incompatible, a third means of verification is required. We have therefore conducted direct numerical simulations of the problem under study, to determine which of the two results is more accurate.

3. Numerical simulations

The numerical simulations conducted here were based on the use of a full Navier–Stokes incompressible front-tracking code developed by Popinet and Zaleski in recent years [28]. The detailed description of the code will not be given here, but can be found in the referenced paper. This code has been shown to yield very accurate results in the prediction of interfaces deformation, particularly in the case of the viscous damping of capillary waves (see Popinet [29]). In the present study, two periodic layers of incompressible viscous fluids separated by a perturbed interface are initially superposed between two horizontal rigid boundaries. The distance between the boundaries is equal to the wavelength of the perturbation (using larger simulation domains does not change the results significantly, which shows that the effect of confinement is negligible). The domain is discretized using a regular cartesian grid (256^2 cells) and an adaptive time-stepping procedure is used to resolve the very short initial time scales. A strong acceleration is imposed for a very short time, and the response of the fluids is simulated. A Fourier transform of the shape of the interface is then calculated, and the first two terms (mode one and two) are compared with formula (6). Note that in order to increase the precision of the simulation of the interface evolution, the dynamic viscosities of the fluids have been chosen equal (see [28,29] for a discussion on this point). The densities however are different, which leads to different kinematic viscosities. The results obtained for several viscosities and several density ratios $\rho^{(1)}/\rho^{(2)}$ are presented in Figs. 2–4 and 5.

Let us define $\eta_v^{[i]}$ as the ith Fourier component (i.e., associated with $\cos(ikx)$) of the non-dimensional interface law (i.e., normalised with respect to η_0), numerically computed for viscous fluids without surface tension. In the same way, let us define $\eta_{v,ST}^{[i]}$ as the ith Fourier component of the non-dimensional interface law numerically computed for viscous fluids with surface tension. Fig. 2 presents $\eta_v^{[1]}$ computed for a density ratio of 2 for several Reynolds numbers (the Reynolds numbers in the figure are calculated for the heavier fluid, the two fluids having by choice the same shear viscosity). The linear inviscid law $(1 + A\Delta V\, kt)$ is also represented. The effect of viscosity is, without surprise, to progressively decrease the growth rate as time elapses, with a stronger and stronger effect as the Reynolds numbers become smaller and smaller.

The precision of the viscous term in Eq. (6) is estimated in Figs. 3(a)–(c) for several Reynolds numbers and three density ratios (2, 4 and 8). In each figure has been plotted the viscous correction, as predicted by the present theory (i.e., the second term of Eq. (6)), as measured in the numerical simulations (i.e., $\eta_v^{[1]} - (1 + A\Delta V\, kt)$) and as predicted by Mikaelian [8] (i.e.,

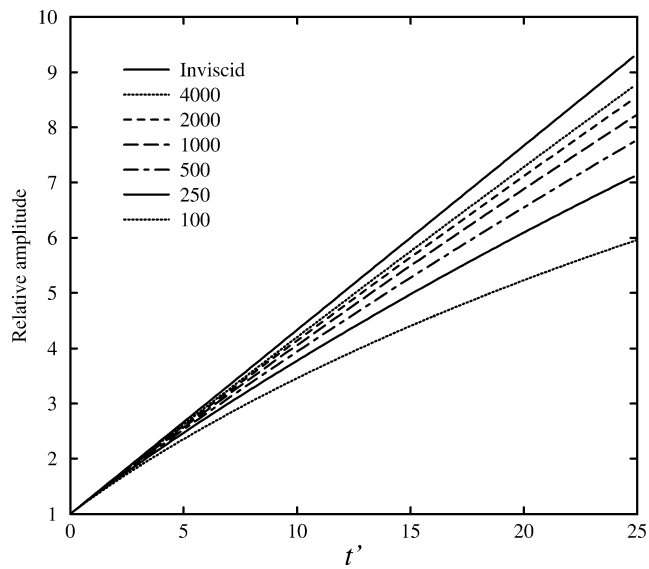

Fig. 2. Amplitude of the interface deformation for a density ratio of 2 and several Reynolds numbers (from 100 to 4000, calculated for the heavier fluid).

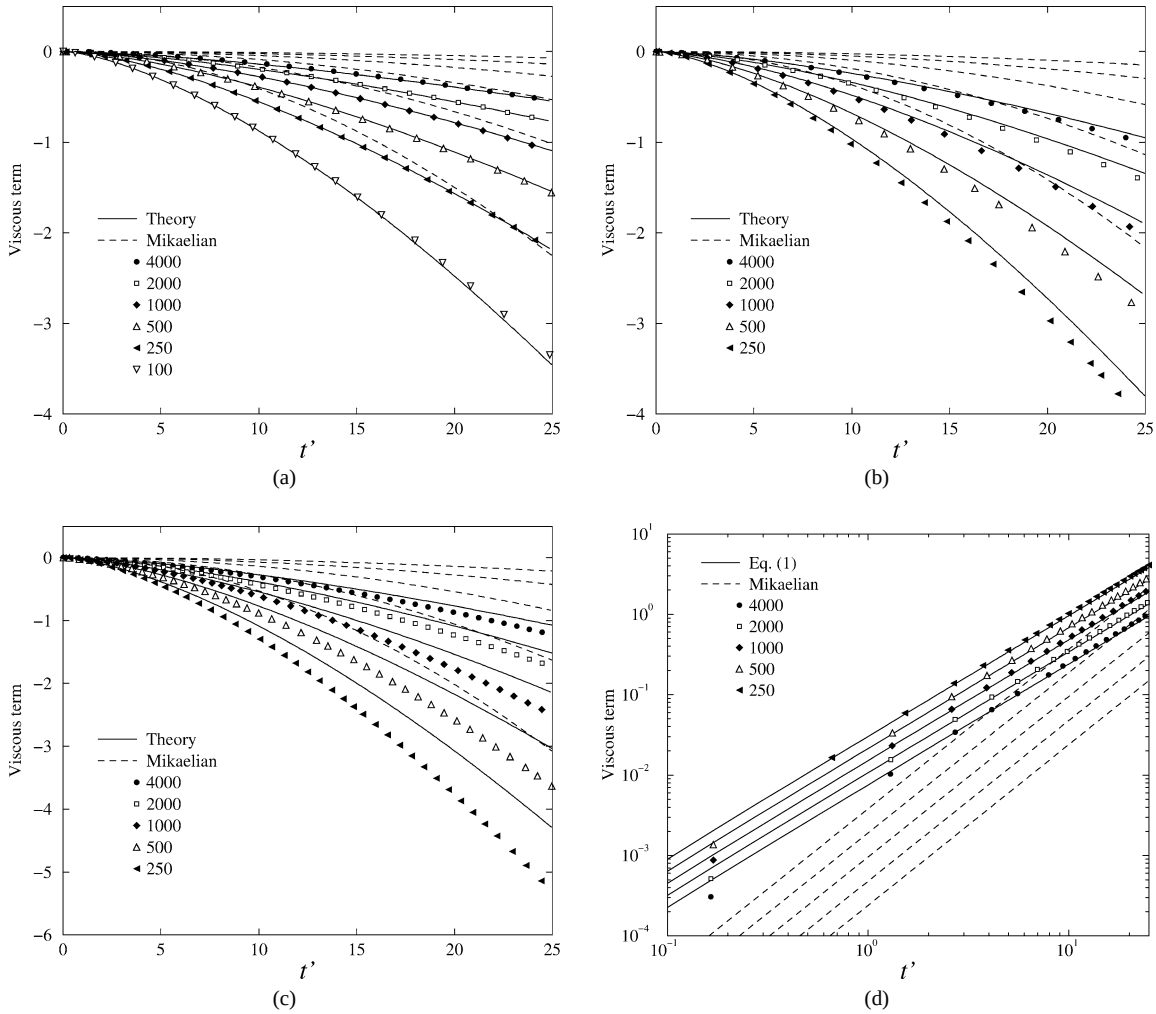

Fig. 3. Viscous correction to the linear growth based on Eq. (6), Eq. (7) (Mikaelian [8]) and numerical simulations for several Reynolds numbers (from 100 to 4000, calculated for the heavier fluid) and several density ratios ((a) $\rho^{(1)}/\rho^{(2)} = 2$, (b) $\rho^{(1)}/\rho^{(2)} = 4$, (c) $\rho^{(1)}/\rho^{(2)} = 8$). (d) Same conditions as in (b) in log–log plot.

Eq. (7) minus $(1 + A\Delta V\, kt)$). In every case, the present theory correctly predicts the effect of viscosity on the interface growth. The precision is excellent in the case of small density ratios, even for large viscosities: for instance, the relative precision of the theoretical viscous correction for $\rho^{(1)}/\rho^{(2)} = 2$ always remains within 2% of the numerical simulation, although the Reynolds numbers are very small in some cases ($\mathrm{Re}^{(1)} = 100$ and $\mathrm{Re}^{(2)} = 50$ in the most viscous case). As the density ratio grows, the precision becomes less and less good, but the theoretical predictions nonetheless remain quantitatively comparable to the simulations: for instance, the theoretical viscous correction remains within 20% of the simulation for $\rho^{(1)}/\rho^{(2)} = 8$ and for the largest viscosity ($\mathrm{Re}^{(1)} = 250$ and $\mathrm{Re}^{(2)} = 31.25$). In every case, the viscous correction as predicted by Mikaelian (Eq. (7)) is far from the results of the simulation, sometimes being even several orders of magnitude smaller. This point is emphasised in Fig. 3(d), where the same data as in Fig. 3(b) (i.e., viscous correction for a density ratio of 4) have been plotted in a log–log diagram. Figs. 3(a)–(d) prove unambiguously that Eq. (7) is inappropriate. A possible explanation of the failure of Mikaelian's theory is linked with the presence of a boundary layer close to the interface, neglected in his approach. In his article indeed, Mikaelian constructs an integral equation linking the vertical velocity $w^{(i)}$ (unknown at this point) and its subsequent derivatives in z to the growth rate of perturbations γ (see Eq. (4) in [8]). An approximate value of γ is then obtained by using an estimated value of $w^{(i)}$, based on the inviscid solution. In other words (and translated into the notations used in the present work), the eigenvalue problem associated to Eq. (4) of [8] is solved using $\varepsilon\overline{w}^{(i)}$ as an approximation for $w^{(i)}$. This choice could seem a reasonnable one at first glance, as $\varepsilon\overline{w}^{(i)}$ is indeed a good approximation of $w^{(i)}$, both in the bulk and in the boundary layer ($w^{(i)} = \varepsilon\overline{w}^{(i)} + \mathrm{O}(\varepsilon^2)$). The relative error made when replacing $w^{(i)}$ by $\varepsilon\overline{w}^{(i)}$ is of order ε, and so it would be tempting to

estimate the relative error made on γ as one of order ε too. This conclusion would be flawed however, as derivatives of $w^{(i)}$ also play a role in the proposed moment equation: a rapid glance at the second order boundary layer expansions presented in the present theory shows that $\varepsilon\overline{w}_z^{(i)}$ is, on the contrary, a very bad approximation of $w_z^{(i)}$ in the boundary layer. The second-order velocity expansion in the boundary layer ($\varepsilon^2\,\widetilde{\widetilde{w}}^{(i)}$) is indeed a function of $\tilde{z}$ and not of z, so that differentiating it along z leads to a term of order ε and not ε^2. In other words, the local contribution to the vertical velocity gradient due to the second-order velocity perturbation is as important as the contribution due to the first order perturbation: one makes a 100% relative error on $w_z^{(i)}$ when replacing it by $\varepsilon\overline{w}_z^{(i)}$. There lies probably the reason of the incorrect result obtained by Mikaelian.

The evolution of the second Fourier mode of the interface is represented on Figs. 4(a)–(c), as predicted by the present theory (i.e., fourth term in Eq. (6)) and as measured on the simulated interface (i.e., $\eta_v^{[2]}$), for the same series of Reynolds numbers and density ratios as in Fig. 3(a)–(c). The numerical simulation does not seem to predict this first non-linear coupling with accuracy when the densities of the fluids are too close: for $\rho^{(1)}/\rho^{(2)} = 2$, some of the numerical curves in Fig. 4(a) seem erratic. This can be explained by the smallness of the non-linear correction in this case: for $t' = 25$, the amplitude of the interface deformation has grown up to 10, while the amplitude of the second mode is still only 0.05 (i.e., 0.5% of the total interface deformation). The numerical scheme is thus unable to resolve with accuracy such a small correction to the shape of the interface. But only a slightly larger density ratio ($\rho^{(1)}/\rho^{(2)} = 4$) is necessary for the code to correctly describe non-linear couplings: for large Reynolds numbers, the numerical curves in Figs. 4(b) and 4(c) seem to converge to the theoretical term, which is equal to the inviscid non-linear correction at the chosen order of asymptotic expansion (see previous section). Note that in Figs. 4(b) and 4(c), this non-linear correction only represents 2 or 3% of the overall amplitude of the interface deformation. These figures

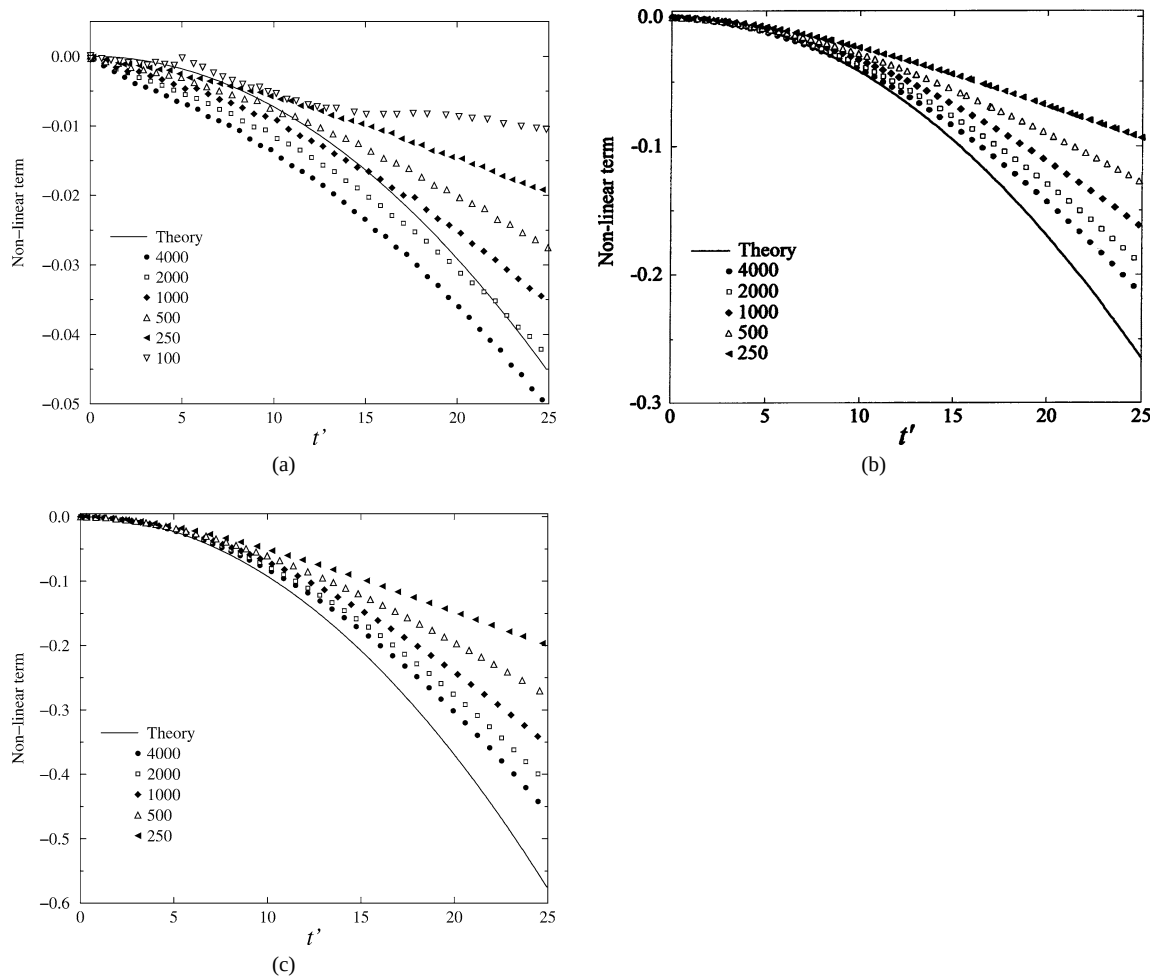

Fig. 4. First non-linear correction based on Eq. (6) and numerical simulations for several Reynolds numbers (from 100 to 4000, calculated for the heavier fluid) and several density ratios. (a) $\rho^{(1)}/\rho^{(2)} = 2$, (b) $\rho^{(1)}/\rho^{(2)} = 4$, (c) $\rho^{(1)}/\rho^{(2)} = 8$.

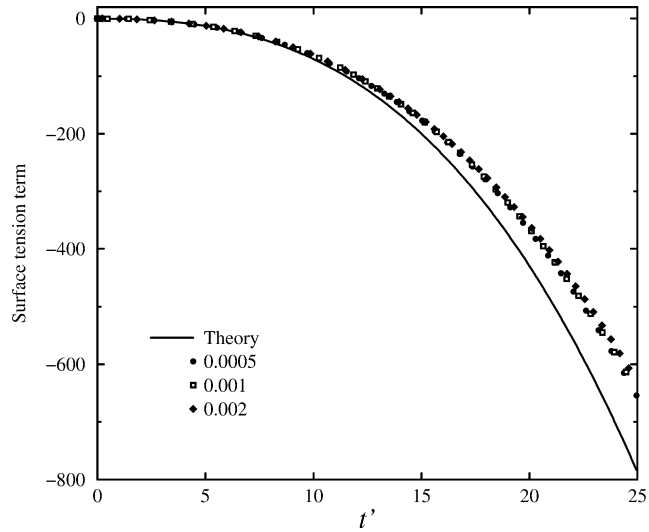

Fig. 5. Normalised correction due to surface tension based on Eq. (6) and numerical simulations for several values of the surface tension.

give an idea of the precision of the numerical scheme as regards the reconstruction of the interface. Although the first non-linear correction presented in Eq. (6) is now a classical result (see, for instance, [15] or [20]), Figs. 4(a)–(c) are to our knowledge its first direct numerical verification. What is remarkable in these comparisons is the importance of viscous effects: the classical inviscid non-linear correction only matches the numerical calculation for very large Reynolds numbers. It was expected to observe a stronger effect of viscosity on the non-linear terms than on the linear one, as non-linear terms have a smaller spatial extension. But the striking result here is the amplitude of this effect: for Reynolds numbers of a few hundreds, inviscid theories over-estimate the first non-linear correction by a factor 4 or even 5. In other words, viscosity not only tends to reduce the global rate of growth of the interface deformation, but it also makes the grown interface more symmetric than in inviscid fluids by limiting the growth of harmonics of the initial deformation.

Finally, Fig. 5 presents the influence of surface tension on the interface growth. The theoretical correction due to surface tension (i.e., the third term in Eq. (6)) is compared to $(\eta_{v,\mathrm{ST}}^{[1]} - \eta_v^{[1]})$ (i.e., the first mode of the interface law obtained in simulations of viscous fluids with surface tension minus the same parameter obtained in simulations without surface tension). Both these sets of values are normalised with respect to the surface tension σ, and plotted for three values of σ. Here again, the comparison between the numerical and the theoretical corrections confirm the validity of Eq. (6). As in the case of viscosity, it would be interesting to analyse numerically the influence of surface tension on the non-linear correction to the interface law: the relative influence of surface tension is expected in this case also to be stronger on the non-linear terms than on the linear one, thus leading to a more symmetric interface.

4. Discussion

The numerical simulations presented in the previous section have confirmed the validity of the theoretical model proposed here. It is now interesting to analyse in more details its characteristics and see how it can be used in a practical context.

As stressed in the previous sections, the main result of this paper is the law of interface deformation given in Eq. (6) and already discussed in the previous section. This law enables to predict in a simple way the relative influence of viscosity, surface tension and non-linearities on the early growth of perturbations on the interface. Of course, as always in such asymptotic treatments, the obtained expansion is secular in time: as time elapses, second-order terms in the interface law grow faster than first-order ones, to eventually become larger. At this point, the asymptotic expansion is no longer valid: non-linear couplings have become of the same order as the linear growth of perturbations, which also means that the perturbations on the interface are now too large to comply with the condition of small interface deformation (i.e., Eq. (1)). Several ways of extending the validity in time of such expansions have been suggested in the past, such as the use of Multiple Time-Scale Analysis [27] or of Padé Approximants [9]. It is beyond the scope of this paper to examine such extensions. However, the proposed law, despite its limited validity in time, can be useful as it is on a practical point of view: for a given experimental setup, application of Eq. (6) in the first moments of the evolution of the interface gives the order of magnitude of each contribution to its deformation (i.e., the linear growth and the corrections due to viscosity, surface tension and non-linear couplings); it therefore permits to rank the

Table 1
Application of Eq. (6) to several experimental cases (the 'Falling bucket' case corresponds to an air/water interface with a perturbation of 5 cm-period and 1 mm-amplitude, submitted to a 4 m/s velocity change); the percentages correspond to the relative value with respect to the linear growth rate $\Delta\mathring{\eta}_L$

Experiment	$t_{\max}$ (ms)	$\Delta\mathring{\eta}_L$ (m/s)	$\Delta\mathring{\eta}_V$ (m/s)	$\Delta\mathring{\eta}_{\mathrm{ST}}$ (m/s)
Jacobs and Niederhaus [26] (water + alcohol/salted water)	62	0.191	0.0042 (2.2%)	0
Jones and Jacobs [24] (N_2/SF_6)	8	1.18	0.0212 (2%)	0
Jacobs and Sheeley run 2 [25] (pure water/salted water)	19	0.328	0.0075 (2.3%)	0
Jacobs and Sheeley run 6 [25] (pure water/salted water)	49	0.138	0.0046 (3.4%)	0
Jacobs and Sheeley run 18 [25] (pure water/salted water)	26	0.196	0.0064 (3.8%)	0
Vetter and Sturtevant [23] (air/SF_6)	0.051	31.1	0.273 (0.9%)	0
Falling bucket	32	0.251	0.00011 (0.04%)	0.016 (6.5 %)

relative influence of these phenomena on the whole evolution. Such an information can be helpful to an experimenter, who can estimate this influence for his or her own experimental setup and choose adequately the theoretical or numerical models to which the experimental data can be confronted (linear or non-linear, with or without surface tension, with or without viscosity). This choice would in this case not be based on ad hoc assumptions (as it is usually the case) but on accurate quantitative arguments.

Such an application has been undertaken here for sets of data recently published by several experimental teams. The following procedure has been used:

Let us define $t_{\max}$ the time after which the interface leaves the weakly non-linear regime. $t_{\max}$ is classically defined as:

$$t_{\max} = \frac{1}{\eta_0 |A| \Delta V\, k^2} \tag{8}$$

(which leads to $\eta/\eta_0 = 1 \pm 1/\varepsilon$ in the linear approximation). Let us call $\Delta\eta$ the 'thickness' of the deformed interface, commonly defined as $(\eta_{\max} - \eta_{\min})/2$. $\Delta\mathring{\eta}$ is thus the rate of growth of the interface deformation. For several experimental configurations, $\Delta\mathring{\eta}$ has been calculated at $t = t_{\max}$ based on Eq. (6). For each calculation, the linear contribution to $\Delta\mathring{\eta}$ (i.e., $A\Delta V\, k$) has been noted $\Delta\mathring{\eta}_L$, the viscous contribution $\Delta\mathring{\eta}_V$ and the contribution due to surface tension $\Delta\mathring{\eta}_{\mathrm{ST}}$. Note that non-linear couplings only influence $\Delta\eta$ at the third order of expansion in ε, not taken into account here. The results of these calculations are summarised in Table 1. The relative values of $\Delta\mathring{\eta}_V$ and $\Delta\mathring{\eta}_{\mathrm{ST}}$ with respect to the linear growth rate $\Delta\mathring{\eta}_L$ give an estimation of the importance of the effect of viscosity and surface tension when the interface enters the non-linear regime (i.e., at $t = t_{\max}$). Two different cases clearly stand: experiments with gases, and experiments with liquids. In experiments with pairs of gases in shock tubes (see Jones and Jacobs [24] and Vetter and Sturtevant [23]), the relative influence of viscosity on the growth rate is typically between one and two percents. This quantitative estimation formally justifies the customary assumption of negligible viscous effects in such experiments: it is expected that the mutual diffusion between the gases is a stronger source of attenuation of the growth rate than viscous stresses. In experiments based on impulsively accelerated pairs of liquids (like in Jacobs and Sheeley [25] or Jacobs and Niederhaus [26]), the picture changes significantly: a relative influence of viscosity of the order of 4% or more is not unusual. In such cases, viscosity becomes a source of perturbation potentially as important (or even more) as mutual diffusion of the two liquids. A great care should therefore be taken in interpreting such data using non-viscous models. Finally, application of the proposed criterion to the 'falling bucket' experiment (i.e., dropping a bucket full of water on the floor) shows that the interface deformation is entirely governed by non-linearities and surface tension: viscosity should play almost no role in problems of impacting liquids like the splashing of a drop on a fluid layer or the impact of a wave on a wharf (see Gueyffier and Zaleski [5,6]).

The law of interface deformation given in Eq. (6) has been studied in depth. But the result of the theoretical analysis is not limited to this law. Indeed, the asymptotic expansions give also access to the pressure and velocity fields in the two fluids, an information which can be of great interest in some cases. For instance, as stressed before, the interface in the RM instability behaves like a shear layer, and as such is subjected to secondary instabilities of the Kelvin–Helmholtz type. Such secondary instabilities, clearly observed in experiments [26] or numerical simulations [22], are responsible for the strong mixing which ensues between the two fluids as a result of their impulsive acceleration. It is expected that the presence of boundary layers on each side of the interface will have a strong influence on the growth rate of these secondary instabilities, so that using non-

viscous models to predict the onset of these would certainly give erroneous estimations. Knowing in details the velocity field is therefore an interesting information.

As an example, the shape of the interface and the velocity field have been drawn in Fig. 6 for the 'falling bucket' experiment: an interface between air and water subjected to a periodic perturbation of 5 cm-period and 1 mm-amplitude, accelerated by 4 m/s in a stable configuration. These parameters typically describe the falling of a bucket full of water on the floor from a

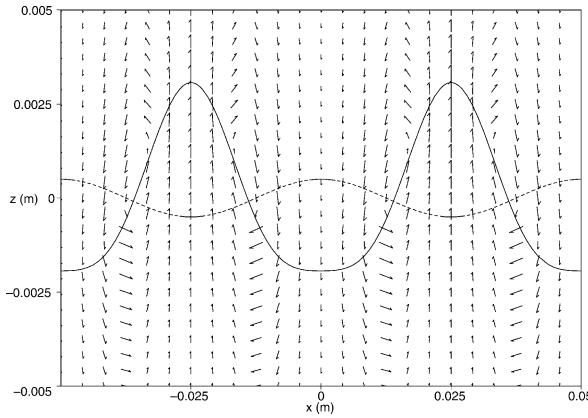

Fig. 6. Shape of the interface and velocity field for the 'falling bucket' experiment, 12 ms after the impact (air/water interface with a perturbation of 5 cm-period and 1 mm-amplitude, submitted to a 4 m/s velocity change).

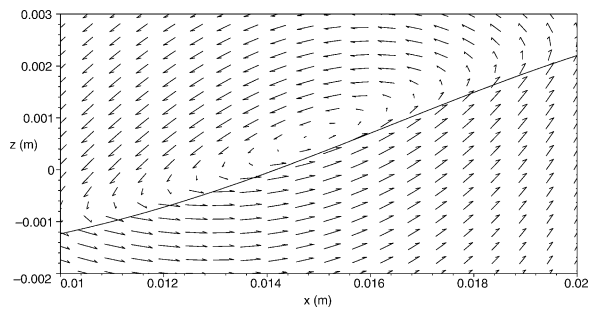

Fig. 7. Zoom on one of the vortices in Fig. 6.

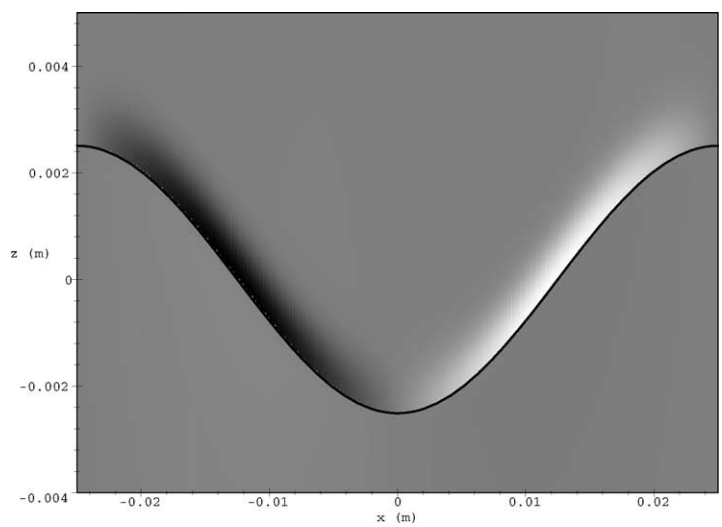

Fig. 8. Vorticity distribution for the same conditions as in Fig. 6 (first-order only).

human's height. The plot in Fig. 6 represents the state of the interface 12 ms after the impact. The characteristic phase inversion of the interface deformation is observed, as well as the typical 'spikes and bubbles' pattern created by non-linear couplings. The velocity field shows how the interface is distorted by two vortices located roughly at the nodes of the initial perturbation. Note that the interface is subjected to a non-zero tangential velocity, as expected in a viscous theory. A closer look at the above mentioned vortices suggests that they are not exactly centered on the interface itself. On Fig. 7, a zoom on one of these vortices clearly shows that the center of the vortex is in fact located in the lighter fluid (air), which is also the more viscous one (in terms of kinematic viscosity): vorticity has diffused preferentially in the most viscous of the two fluids, leaving water almost free of vorticity. This conclusion is confirmed by a vorticity plot for the same parameters, presented in Fig. 8: vorticity has diffused largely in the gas phase, whereas the liquid phase remains almost irrotational.

5. Conclusion

In this paper, we propose a new weakly non-linear theoretical model of the Richtmyer–Meshkov instability between two viscous fluids with surface tension in a 2D geometry. The model is based on the application of singular perturbations techniques to the incompressible Navier–Stokes equations written for two superposed immiscible fluids. A simple analytical law of interface deformation is obtained, in which the effects of viscosity, surface tension and non-linearities appear under the form of independent terms. This law compares well with accurate direct numerical simulations we performed using an in-house numerical code. The proposed law should give a precise quantitative estimation of the relative influence of the three above mentioned effects when applied to any given experimental setup. It can consequently be used as a tool by experimenters to estimate whether side-effects like viscosity or surface tension have to be considered in the interpretation of their data. A first series of such estimations on published sets of data shows that the influence of viscosity on the growth rate of perturbations in typical shock-tube experiments is often less than 1%, justifying the assumption of negligible viscous effects usually made in such configurations. At the same time however, estimations show also that the rates of growth measured in experiments with impulsively accelerated liquids are sometimes influenced to the extent of a few percents by viscosity, so that the use of non-viscous models for their interpretation is more questionnable. Finally, the model gives also access to the pressure and velocity fields in both fluids. This result enables in particular to have a precise estimation of the distribution of vorticity in the fluids, an information which can be of great interest for the study of secondary Kelvin–Helmholtz instability.

Acknowledgements

The authors wish to acknowledge Pr. Stéphane Zaleski and Dr. Christophe Josserand from Laboratoire de Modélisation en Mécanique (Université Paris 6, France) for stimulating discussions.

References

[1] R.D. Richtmyer, Taylor instability in shock acceleration of compressible fluids, Comm. Pure Appl. Math. 13 (1960) 297–319.
[2] E.E. Meshkov, Instability of the interface of two gases accelerated by a shock wave, Fluid Dyn. 43 (5) (1969) 101–104.
[3] M.H. Anderson, B.P. Puranik, J.G. Oakley, P.W. Brooks, R. Bonazza, Shock tube investigation of hydrodynamic issues related to inertial confinement fusion, Shock Waves 10 (2000) 377–387.
[4] D. Arnett, B. Fryxell, E. Muller, Instabilities and nonradial motion in SN 1987 A, Astrophys. J. Lett. 341 (1989) 63.
[5] D. Gueyffier, S. Zaleski, Formation de digitations lors de l'impact d'une goutte sur un film liquide, C. R. Acad. Sci. Paris, Série IIb 326 (1998) 839–844.
[6] D. Gueyffier, Étude de l'impact de gouttes sur un film liquide mince, Ph.D. Thesis, Université Pierre et Marie Curie, Paris 6, 2000.
[7] K.O. Mikaelian, Rayleigh–Taylor and Richtmyer–Meshkov instabilities in multilayer fluids with surface tension, Phys. Rev. A 42 (12) (1990) 7211–7225.
[8] K.O. Mikaelian, Effect of viscosity on Rayleigh–Taylor and Richtmyer–Meshkov instabilities, Phys. Rev. E 47 (1) (1993) 375–383.
[9] Q. Zhang, S.I. Sohn, An analytical nonlinear theory of Richtmyer–Meshkov instability, Phys. Lett. A 212 (1996) 149–155.
[10] A.L. Velikovich, G. Dimonte, Nonlinear perturbation theory of the incompressible Richtmyer–Meshkov instability, Phys. Rev. Lett. 76 (17) (1996) 3112–3115.
[11] P. Carlès, S. Popinet, Viscous nonlinear theory of Richtmyer–Meshkov instability, Phys. Fluids 13 (7) (2001) 1833–1836.
[12] Y. Yang, Q. Zhang, D. Sharp, Small amplitude theory of Richtmyer–Meshkov instability, Phys. Fluids 6 (5) (1994) 1856–1873.
[13] A.L. Velikovich, Analytic theory of Richtmyer–Meshkov instability for the case of reflected rarefaction wave, Phys. Fluids 8 (6) (1996) 1666–1679.
[14] J.G. Wouchuck, K. Nishihara, Linear perturbation growth at a shocked interface, Phys. Plasmas 3 (10) (1996) 3761–3776.

[15] M. Berning, A.M. Rubenchik, A weakly nonlinear theory for the dynamical Rayleigh–Taylor instability, Phys. Fluids 10 (7) (1998) 1564–1587.
[16] K.A. Meyer, P.J. Blewett, Numerical investigation of the stability of a shock-accelerated interface between two fluids, Phys. Fluids 15 (5) (1971) 753–759.
[17] K.O. Mikaelian, Growth rate of the Richtmyer–Meshkov instability at shocked interfaces, Phys. Rev. Lett. 71 (18) (1993) 2903–2906.
[18] M. Vandenboomgaerde, C. Mügler, S. Gauthier, Impulsive model for the Richtmyer–Meshkov instability, Phys. Rev. E 58 (2) (1998) 1874–1882.
[19] O.A. Hurricane, E. Burke, S. Maples, M. Viswanathan, Saturation of Richtmyer's impulsive model, Phys. Fluids 12 (8) (2000) 2148–2151.
[20] Q. Zhang, S.I. Sohn, Nonlinear theory of unstable fluid mixing driven by shock wave, Phys. Fluids 9 (4) (1997) 1106–1124.
[21] M. Vandenboogaerde, S. Gauthier, C. Mügler, Nonlinear regime of multimode Richtmyer–Meshkov instability: a simplified perturbation theory, Phys. Fluids 14 (3) (2002) 1111.
[22] A.D. Kotelnikov, J. Ray, N.J. Zabusky, Phys. Fluids 12 (12) (2000) 3245.
[23] M. Vetter, B. Sturtevant, Experiments on the Richtmyer–Meshkov instability of an air/SF_6 interface, Shock Waves 4 (1995) 247–252.
[24] M.A. Jones, J.W. Jacobs, A membraneless experiment for the study of Richtmyer–Meshkov instability of a shock-accelerated gas interface, Phys. Fluids 9 (10) (1997) 3078–3085.
[25] J.W. Jacobs, J.M. Sheeley, Experimental study of incompressible Richtmyer–Meshkov instability, Phys. Fluids 8 (2) (1996) 405–415.
[26] J.W. Jacobs, C.E. Niederhaus, PLIF flow visualization of single and multimode incompressible Richtmyer–Meshkov instability, in: Proc. 6th International Workshop on the Physics of Compressible Turbulent Mixing, Marseille, France, 18–21 June 1997, 1997, pp. 214–219.
[27] J. Kevorkian, J.D. Cole, Perturbation Methods in Applied Mathematics, Springer-Verlag, 1981.
[28] S. Popinet, S. Zaleski, A front-tracking algorithm for accurate representation of surface tension, Int. J. Numer. Methods Fluids 30 (1999) 775–793.
[29] S. Popinet, Stabilité et formation de jets dans les bulles cavitantes : développement d'une méthode de chaîne de marqueurs adaptée au traitement numérique des équations de Navier–Stokes avec surfaces libres, Ph.D. Thesis, Université Pierre et Marie Curie, Paris 6, 2000.